Bidirectional Asymmetric Frequency Conversion in Nonlinear Phononic Crystals

Yeongtae Jang,[1,*] Beomseok Oh,[1,*] Eunho Kim,[2,3,4,†] and Junsuk Rho[1,5,6,7,‡]
[1]Department of Mechanical Engineering, Pohang University of Science and Technology (POSTECH), Pohang 37673, Republic of Korea
[2]Division of Mechanical System Engineering, Jeonbuk National University, Jeonju, 54896, Republic of Korea
[3]Department of JBNU-KIST Industry-Academia Convergence Research, Jeonju, 54896, Republic of Korea
[4]Graduate School of Mechanical-Aerospace-Electric Convergence Engineering, Jeonbuk National University, Jeonju 54896, Republic of Korea
[5]Department of Chemical Engineering, Pohang University of Science and Technology (POSTECH), Pohang 37673, Republic of Korea
[6]Department of Electrical Engineering, Pohang University of Science and Technology (POSTECH), Pohang 37673, Republic of Korea
[7]POSCO-POSTECH-RIST Convergence Research Center for Flat Optics and Metaphotonics, Pohang 37673, Korea

(Received 17 August 2024; accepted 16 June 2025; published 15 July 2025)

Beyond conservative systems, altering the wave propagation frequency emerges as a crucial factor across diverse physical domains. This Letter presents a demonstration of bidirectional asymmetric frequency conversion—either upward or downward—depending on the excitation direction, surpassing conventional unidirectional mechanisms. We numerically and experimentally demonstrate its practical realization in a model system of cylindrical granular crystals with intrinsic local resonance coupling. This novel wave transport mechanism arises from the interplay of nonlinear contact, spatial asymmetry, and coupled local resonance. In particular, we show that local resonance coupling induces wavenumber-dependent wave dynamics, including frequency conversion. Given that this local resonance exemplifies avoided crossings (i.e., strong coupling), this Letter may inspire studies on nonlinear systems supporting material or structural resonance.

DOI: 10.1103/3n97-7kmd

One of the fundamental elements of wave propagation is frequency, which dictates how waves interact with matter. In a closed linear system, the laws of energy and momentum conservation stemming from time-reversal symmetry prevent the alteration of the assigned frequency. Therefore, changing the frequency allows us to overcome physical constraints such as reciprocity [1], the diffraction limit [2–4], and energy localization [5]. As a result, frequency conversion has garnered considerable attention across diverse wave dynamics domains [6–10].

To break the time-invariant property of wave propagation, various principles have been put forward and successfully applied. Examples range from utilizing external bias [11–13] or time-varying media [14,15], to exploiting external coupling (such as optomechanical interactions [16]) or nonlinear effects [17–19]. Among these approaches, leveraging nonlinearity is particularly advantageous because it enables the straightforward tuning of the desired frequency by adjusting the wave amplitude.

Expanding on basic frequency conversion, recent studies in phononics have demonstrated not only frequency alteration but also simultaneous asymmetric wave transmission using various nonlinear effects [20–25]. These advancements have significantly promoted innovative applications, including acoustic diodes [26,27], switching [28], and logic gates [29]. Typically, these wave transfers are achieved using structures that introduce internal defects and heterostructures to break spatial symmetry [23,24,28–30]. By doing so, the system enables the definitive frequency conversion upward or downward in one direction while inhibiting wave transmission in the opposite direction. However, this frequency conversion remains constrained to a unidirectional process.

Building upon this phenomenon, we posed the question: Can we realize asymmetric frequency conversion depending on the direction of excitation within the same system?. This pursuit promises more freedom in wave manipulation, driving the motivation behind this Letter. Indeed, a similar wave transfer concept was initially proposed for quantum-level nonlinear devices using parametric biharmonic pumps [31]. However, achieving this phenomenon requires sophisticated wave mixing, and experimental realization remains a challenge yet to be fully realized.

In this Letter, we demonstrate bidirectional asymmetric frequency conversion (BiAFC) in cylindrical granular crystals composed of slender cylindrical beams interacting via nonlinear Hertz contact [32,33]. These discrete architectures are highly tunable and can demonstrate a plethora of wave physics, ranging from linear to strongly nonlinear

*These authors contributed equally to this work.
†Contact author: eunhokim@jbnu.ac.kr
‡Contact author: jrsho@postech.ac.kr

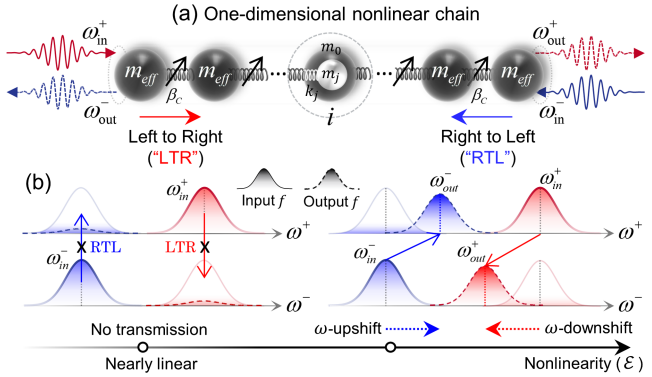

FIG. 1. Bidirectional asymmetric frequency conversion. (a) A one-dimensional locally resonant spring-mass chain, where neighboring cells interact through a nonlinear potential. This nonlinear chain features broken spatial symmetry and local resonance. Gaussian wave-packet propagation in the (+) direction (left to right, LTR) and (−) direction (right to left, RTL). (b) Wave transport scenarios, depending on whether the system exhibits nonlinearity. Solid (dashed) lines indicate the input (output) frequency spectrum. Left: bidirectional prohibition of wave transmission in the linear regimes. Right: bidirectional asymmetric wave transfer with frequency conversion in the nonlinear regimes.

behavior [34–39]. What makes the use of slender cylindrical elements special compared to classical granular media (e.g., spherical or thick elements) is the phenomenon of "local resonance coupling," where structural resonances lead to hybridization and mode splitting, as typically observed in strong mode coupling frameworks. Our primary finding is that the interplay among nonlinearity, local resonance, and graded spatial variation enables BiAFC, where the assigned frequency undergoes either up-conversion or down-conversion depending on the excitation direction within the same system. Furthermore, our Letter reveals that local resonance coupling gives rise to wavenumber-dependent wave dynamics, including frequency conversion.

Schematic arguments—The underlying mechanism of the BiAFC is schematically depicted in Fig. 1. To begin with a general discussion in phononics, we consider a generic locally resonant spring-mass system [Fig. 1(a)]. The neighboring cells interact through a nonlinear spring indicated by inclined arrows. This nonlinear chain features broken spatial symmetry along with local resonance. Gaussian-modulated waveforms are applied as the input, with wave propagation direction set as (+) for left to right (LTR) and (−) for right to left (RTL).

Wave transport in this system can appear in two distinct ways, reliant on whether the system exhibits nonlinearity: when subjected to small-amplitude excitation, the system is limited to linear dynamics, which results in the bidirectional prohibition of wave transmission [see Fig. 1(b)]. However, as the amplitude increases, nonlinear interactions between the particles may enable wave transmission. Notably, the nonlinear effects also give rise to the frequency conversion [see Fig. 1(b)], which exhibits frequency shifts upward or downward depending on the direction of incidence. More specifically, in RTL (LTR) propagation, a Gaussian-modulated pulse centered at ω_{in}^{-} (ω_{in}^{+}) experiences an up (down) shift, while LTR (RTL) transmission is restricted at ω_{in}^{-} (ω_{in}^{+}). This novel wave transport is realized in macroscale phononic crystals, as we demonstrate in the following.

Experimental and theoretical setups—For the proposed concept, achieving a tunable local resonance within a unit cell is crucial. We achieve this by utilizing cylindrical beam crystals as shown in Fig. 2(a). In such a system, the local resonance is "intrinsic" (i.e., the vibrational bending mode of the continuum beam itself [40]), which enables seamless tuning of the resonant frequencies by adjusting the length (L) of the cylindrical beam. Each cylinder, made of fused quartz, contacts its center orthogonally with the adjacent cylinders. Our elastic chain consists of 31 cylinders with lengths gradually varying from 90 to 110 mm while maintaining their diameters. This spatially asymmetric chain leads to asymmetric local resonance due to the relationship of $\omega \propto 1/L^2$ [41]. By applying a precompression ($F_0 = 5$ N), we form a packed ensemble of cylindrical beams. The guide rods ensure out-of-plane oscillation of the beam. We then excite a Gaussian-modulated wave into the chain through a piezoelectric actuator for either direction, i.e., LTR (ω_{in}^{+}) or RTL (ω_{in}^{-}). The particle velocity of each beam near the contact point is measured using a laser Doppler vibrometer (Polytec; OFC-534) mounted on a linear stage. Details of the experiments and data acquisition are provided in Supplemental Material [42], Sec. I.

The wave dynamics of the cylinder chain along the axes of the contacts are investigated using a discrete element model. In this approach, we represent single cylindrical beams by a primary point mass (m_0) with multiple resonators [Fig. 2(b)]. The internal resonators consist of local spring (k_j) and mass (m_j), where j represents the number of modes. The parameter of a discretized unit cell is obtained using a physics-informed discrete element modeling approach [43], rooted in continuum beam theory and wave dynamics within periodic structures. Thus, it simplifies the dynamic calculation process efficiently while maintaining analytical accuracy. Detailed mathematical modeling is provided in Supplemental Material [42], Secs. II.A and B.

The unit cells interact through nonlinear potential, and their behavior is governed by Hertz contact [32]. The contact force between the (i)th and $(i+1)$th beam can be written as $F = \beta_c[\delta_i + u_i - u_{i+1}]_+^{3/2}$, where β_c is the stiffness coefficient, and δ_i is the initial displacement due to the F_0; the bracket $[\cdot]_+ = \max(\cdot, 0)$ indicates that it only supports compressive forces, not tensile forces. As indicated by the contact force formula, the system's nonlinearity is adjusted by varying the dynamic and

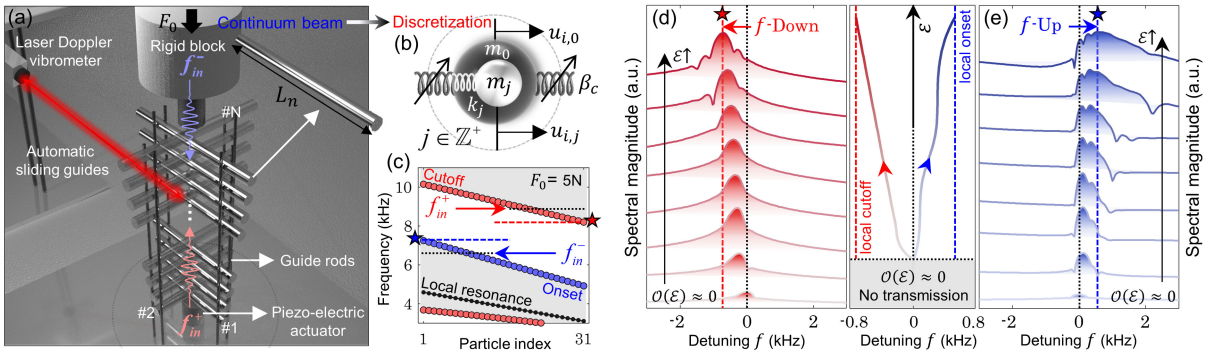

FIG. 2. Wave dynamics from linear to nonlinear regimes. (a) Schematic of the experimental setup. (b) Theoretical discretized unit cell representing a single cylindrical element; see the main text for details. (c) Quasiband diagram obtained from the boundary edges of the dispersion curve for each unit cell. The white area denotes passband regimes, and the gray area denotes the local resonance band gap. Frequency response as wave amplitude increases for (d) LTR excitation and (e) RTL excitation. As the system's nonlinearity increases, the LTR direction undergoes frequency down-conversion, while the RTL direction exhibits frequency up-conversion (i.e., BiAFC). The converted frequencies converge to the local eigenfrequencies (red and cyan stars). The middle panel summarizes the detuning frequency for both upward and downward conversions.

static displacements: from linear regimes when $|u_i - u_{i+1}| \ll \delta_i$ to nonlinear regimes when $|u_i - u_{i+1}| \gtrsim \delta_i$ (see Supplemental Material [42], Sec. II.C for detailed numerical simulations).

Linear spectrum—We first consider the linear dynamics. Based on the discretized building blocks, it is straightforward to identify a group of local eigenstates, i.e., *quasiband*. In Fig. 2(c), we show the quasiband diagram of our gradient-index cylinder chain, focusing on the vicinity of the first resonance band. This quasiband is constructed from characteristic frequencies extracted at the edges of the dispersion curves: the onset frequency at $k = 0$, the cutoff frequency at $k = \pi$, and the local resonance frequency at $k = -i\infty$ (see Supplemental Material [42], Sec. II, for details). The shaded gray area represents a local resonance-induced band gap.

Wave dynamics—We now investigate wave dynamics across a range of small (linear) to large (nonlinear) amplitude excitations. In our setup, we assign Gaussian-modulated center frequency $f_{\text{in}}^+ = 8.92$ kHz and $f_{\text{in}}^- = 6.63$ kHz. In Figs. 2(d) and 2(e), we show the evolution of the frequency spectrum of the output as the system's nonlinearity increases in the LTR and RTL directions. The plot shown between those in Figs. 2(d) and 2(e) summarizes the detuning frequency trends as the system nonlinearity increases.

In the linear limits, the driven frequency encounters the band gap in both directions, as depicted in the quasiband [red and cyan arrows in Fig. 2(c)]. This prevents waves from propagating to the end of the chain and inhibits frequency conversion as well. Yet, an important point is that, for a Gaussian-modulated wave input, the spatiotemporal map reveals a boomerang-shaped wave motion. This distinctive motion leads to *local wave amplification* within the system. It should be noted that such characteristics generally arise in spatial gradient systems [49–51] due to variations in the propagating group velocity and are commonly referred to as "gradons" in various fields [44,45,52]. Comprehensive numerical and experimental findings on this wave motion are provided in Supplemental Material [42], Sec. III (e.g., Figs. S4, S5, and Movies S1, S2).

Along with local wave amplification, a further increase in amplitude can induce nonlinear effects within the system. Therefore, the wave packet can reach the end of the chains beyond linear limits, i.e., the penetration of the band gap. Moreover, a frequency conversion is observable: down-conversion in the LTR direction and up-conversion in the RTL direction, referred to as BiAFC. Frequency conversion becomes even more evident for large amplitudes. The full 2D spectrum map is available in Supplemental Material [42], Sec. IV. Remarkably, the final asymmetric converted frequencies in both directions are saturated at specific local frequencies, indicated by red and cyan stars. These local frequencies are akin to the onset and cutoff frequencies of the first (#1) and last (#31) elements observed in the quasiband [Fig. 2(c)]. This is because, despite the perturbations caused by nonlinearity, the dominant spectrum firmly remains rooted in the linear basis. This implies that the input wave packet frequencies can follow the trajectories of the asymmetric local eigenstates in the form of spatially extended modes in nonlinear regimes. In colloquial terms, the assigned frequencies undergo "climbing" or "descending" quasibands, which depend on the excitation direction. Notably, these dynamics do not require traditional wave-mixing techniques [18,53], paving the way for a more straightforward and direct energy conversion process.

The study of these extended modes traces back to prior literature [24], which explored asymmetric wave transmission (i.e., nonreciprocity) in classical granular crystals, demonstrating unidirectional frequency down-conversion. However, the novelty of our Letter lies in demonstrating

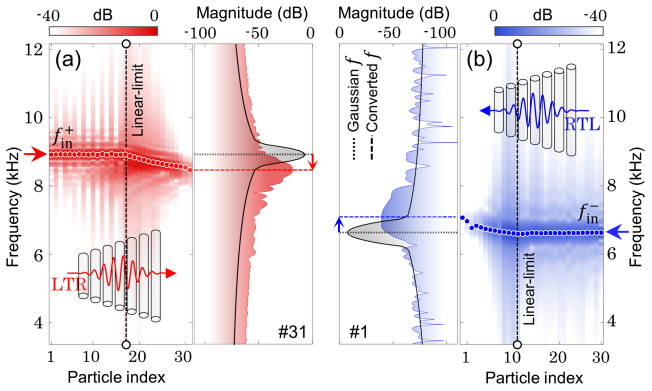

FIG. 3. Experimental validation of bidirectional and asymmetric frequency conversion. Spatial-frequency map for (a) downward conversion (LTR direction) and (b) upward conversion (RTL direction), obtained by calculating the Fourier transform of particle velocity along the chain. The local peak values of the spectral magnitude are highlighted by circles within the chains. The right panel in (a) and the left panel in (b) display the converted-frequency spectrum of the last cylinders for each direction (No. 31 for LTR and No. 1 for RTL).

bidirectional asymmetric frequency transformation. This remarkable achievement is attributed to our strategic use of *local resonance* bands. Thus, in principle, BiAFC could be extended to multiple modes through a more systematic design of the beam element, given the infinite number of modes inherent to a continuum system [41].

Experimental demonstration—Now, we experimentally demonstrate this wave phenomenon in our cylindrical granular crystal. We excite the first cylinder of the chain in the LTR (f_{in}^{+}) and RTL (f_{in}^{-}) directions by driving the actuator with a high amplitude to invoke nonlinearity. In Figs. 3(a) and 3(b), we show spatial-frequency maps by performing the Fourier transformation of each particle's velocity within the chains. In these maps, we track the local frequencies with the maximum spectral magnitude (indicated by circles) along the chain. Even beyond the linear limits (dotted lines) defined by the quasibands, distinct frequency components emerge. Moreover, we observe that the input frequency remains unchanged up to the linear limit, indicating that nonlinear effects are minimal within this regime. This indicates that the primary nonlinear effects arise within the system, specifically near the linear limits, where local wave amplification occurs (as evidenced by the sudden broadening of spectral intensity near the linear limit in Fig. 3). Thus, the nonlinear effects within the system can guide the extended frequency components to transition smoothly to the next eigenstate while avoiding the band gap. This transition process recurs until the wave packet reaches the end of the chain, and this observation supports the previously argued concepts of climbing or descending frequencies. We further support this argument by performing short-time Fourier transforms (see Supplemental Material [42], Sec. IV). However, at extremely high excitation amplitudes, nonlinear distortions emerge from the very beginning of the system, potentially leading to chaotic bands.

The final converted-frequency spectrum (f_{out}^{+} and f_{out}^{-}) of the last cylinder (#31 and #1) is shown in the right panel of Fig. 3(a) and the left panel of Fig. 3(b). A key finding in this spectral comparison is the *wavenumber-dependent* frequency conversion phenomenon, which exhibits a distinct asymmetry: down-conversion results in a narrow bandwidth with higher amplitude, while up-conversion leads to a broader bandwidth with lower amplitude. This asymmetry arises because the strength of the nonlinear interactions, stemming from the system's discreteness, varies with the wavelength. In down-conversion, short-wavelength modes experience stronger nonlinear interactions, enhancing the nonlinear effect but confining the frequency range. In contrast, up-conversion involves long-wavelength modes extending over a broader spatial region, enabling a wider frequency range; however, as the energy is distributed over a larger domain, the amplitude remains lower. This wavenumber-dependent frequency conversion enables control over spectral characteristics. Compared to conventional methods with limited conversion ranges, it allows for the adjustment of a broader range of frequency components, offering enhanced flexibility for diverse applications. In this regard, we also highlight our observations in *linear* wave propagation, including resonance gradons and damping forces exhibiting wavenumber-dependent behavior, as detailed in Supplemental Material [42].

Effects of asymmetry—Next, we examine key parameters—the system's gradient profile—for tunable frequency conversion in a controllable manner. Our analytical modeling enables straightforward exploration of various bidirectional control methods. To examine the influence of the gradient profile, we define an asymmetry factor α, which quantifies the slope of the quasiband profiles, $\alpha = (\alpha_{\text{c}} + \alpha_{\text{s}})/2$ with $\alpha_{\text{c}} = |f_{\text{c},1} - f_{\text{c,N}}|/f_{\text{c,cen}}$ and $\alpha_{\text{s}} = |f_{\text{s},1} - f_{\text{s,N}}|/f_{\text{s,cen}}$, where $f_{\text{c(s)},1}$, $f_{\text{c(s)},\text{cen}}$, $f_{\text{c(s)},\text{N}}$ indicate the cutoff (onset) frequencies of first, center, and last cylinder (see Fig. 4). To create a linearly sloped eigenstate profile, we fix the eigenfrequency of the central cylinder.

In Fig. 4(a), we depict a schematic of potential wave transmission (and conversion) scenarios based on the degree of slope. For a symmetric configuration with $\alpha = 0$, (i.e., a homogeneous chain), bidirectional wave transmission can occur within the passband under the given excitation [see the black arrow in Fig. 4(a)] without frequency change. Initially, as α increases slightly from 0, BiAFC is achieved following asymmetric eigenstates, and with further elevation of the gradient, tunable frequency conversion becomes possible. Yet, with α becoming very large, wave transmission, as well as frequency conversion, becomes unattainable for bidirectional excitation.

To further verify this situation, we perform a full numerical simulation on our given chain by increasing

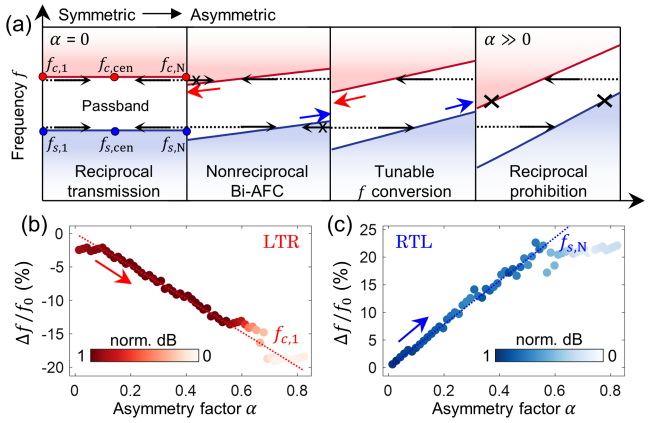

FIG. 4. Effects of the asymmetric chain configuration on frequency conversion. (a) Schematic illustration of wave transport scenarios to the asymmetry factor α. Each panel shows a quasiband diagram for increasing α, with black arrows indicating the excitation frequency and direction. Numerical results of fractional detuning frequency ($\Delta f/f_0$) and normalized decibel magnitude for (b) down-conversion (LTR) and (c) up-conversion (RTL) as a function of α. The red (cyan) dotted line indicates the predicted cutoff (onset) frequency $f_{c,1}(f_{s,N})$, at the last cylinder for each configuration.

the asymmetry factor. In Figs. 4(b) and 4(c), we present the detuning frequency, expressed as a percentage relative to the excitation frequency, for both LTR and RTL directions. The color indicates the normalized magnitude of the Fourier intensity. As the system's slope increases, we observe a steady increase in the converted frequency in both directions. Notably, our conversion mechanism shows that the final converted frequency saturates with minimal deviation at $f_{c,1}$ in the LTR direction and at $f_{s,N}$ in the RTL direction. This implies that, as previously mentioned, the assigned frequencies undergo a gradual climbing or descending process, eventually reaching the final eigenstates in each direction. When the asymmetry factor becomes very large, frequency conversion becomes less well-defined for a given excitation amplitude. This is because frequency perturbations induced by nonlinearity generally occur relative to the linear basis, and the significant eigenstate intervals, caused by large asymmetry factors, limit the transmission of weak frequency components.

Conclusion—We have demonstrated a novel frequency conversion phenomenon in cylindrical granular crystals, exhibiting bidirectional asymmetric conversion—either upward or downward—depending on the excitation direction. This novel wave phenomenon arises from the interplay among systems' nonlinearity, spatial asymmetry, and local resonance coupling. In particular, we show the wavenumber-dependent nature of frequency conversion induced by local resonance coupling, which offers flexibility in tailoring the converted spectrum. Moreover, propagation behavior can be tuned in a controllable manner simply by adjusting the local resonant frequency, paving the way for diverse applications. This would include the development of bidirectional functional devices with potential uses in vibration filtering, wave rectification, logic operations, and advanced signal processing. Since the local resonance coupling in our system exemplifies a strong coupling effect [54], we believe this Letter naturally extends to diverse domains involving material and structural resonances, including polaritons [55], photonics, and metamaterials, offering new opportunities for advanced energy manipulation.

Acknowledgments—This work was financially supported by the POSCO-POSTECH-RIST Convergence Research Center program funded by POSCO, and the National Research Foundation (NRF) grant (RS-2024-00356928) funded by the Ministry of Science and ICT (MSIT) of the Korean government. B. O. acknowledges the NRF Ph.D. fellowship (RS-2024-00409956) funded by the Ministry of Education (MOE) of the Korean government.

[1] H. Nassar, B. Yousefzadeh, R. Fleury, M. Ruzzene, A. Alù, C. Daraio, A. N. Norris, G. Huang, and M. R. Haberman, Nat. Rev. Mater. **5**, 667 (2020).
[2] D. Rugar, J. Appl. Phys. **56**, 1338 (1984).
[3] J. Zhong, C. Hu, K. Wang, J. Ji, T. Zhuang, H. Zou, J. Lu, H. Heo, B. Liang, Y. Jing, and J.-C. Cheng, Phys. Rev. Lett. **131**, 234001 (2023).
[4] B. Oh, C. Kim, D. Lee, J. Rho, and W. Moon, Ultrasonics **131**, 106933 (2023).
[5] S. Flach and C. Willis, Phys. Rep. **295**, 181 (1998).
[6] M. Jain, H. Xia, G. Y. Yin, A. J. Merriam, and S. E. Harris, Phys. Rev. Lett. **77**, 4326 (1996).
[7] R. Tyumenev, J. Hammer, N. Y. Joly, P. S. J. Russell, and D. Novoa, Science **376**, 621 (2022).
[8] I. Martin, G. Refael, and B. Halperin, Phys. Rev. X **7**, 041008 (2017).
[9] M. Notomi and S. Mitsugi, Phys. Rev. A **73**, 051803(R) (2006).
[10] L. Cortes-Herrera, X. He, J. Cardenas, and G. P. Agrawal, Phys. Rev. A **106**, 023517 (2022).
[11] Q. Wu, X. Zhang, P. Shivashankar, Y. Chen, and G. Huang, Phys. Rev. Lett. **128**, 244301 (2022).
[12] M. Henstridge, M. Först, E. Rowe, M. Fechner, and A. Cavalleri, Nat. Phys. **18**, 457 (2022).
[13] C. Zhang, X. Jiang, and D. Ta, Phys. Rev. Lett. **132**, 114001 (2024).
[14] K. Lee, J. Son, J. Park, B. Kang, W. Jeon, F. Rotermund, and B. Min, Nat. Photonics **12**, 765 (2018).
[15] B. Apffel and E. Fort, Phys. Rev. Lett. **128**, 064501 (2022).
[16] W. Chen, P. Roelli, H. Hu, S. Verlekar, S. P. Amirtharaj, A. I. Barreda, T. J. Kippenberg, M. Kovylina, E. Verhagen, A. Martínez, and C. Galland, Science **374**, 1264 (2021).
[17] A. H. Nayfeh and D. T. Mook, *Nonlinear Oscillations* (John Wiley & Sons, New York, 2008).
[18] M. M. Fejer, Phys. Today **47**, No. 5, 25 (1994).

[19] T. Stolt, J. Kim, S. Héron, A. Vesala, Y. Yang, J. Mun, M. Kim, M. J. Huttunen, R. Czaplicki, M. Kauranen, J. Rho, and P. Genevet, Phys. Rev. Lett. **126**, 033901 (2021).
[20] S. Lepri and G. Casati, Phys. Rev. Lett. **106**, 164101 (2011).
[21] X.-F. Li, X. Ni, L. Feng, M.-H. Lu, C. He, and Y.-F. Chen, Phys. Rev. Lett. **106**, 084301 (2011).
[22] W. Zhou, X. Li, Y. Wang, W. Chen, and G. Huang, J. Sound Vib. **413**, 250 (2018).
[23] T. Devaux, V. Tournat, O. Richoux, and V. Pagneux, Phys. Rev. Lett. **115**, 234301 (2015).
[24] E. Kim, R. Chaunsali, and J. Yang, Phys. Rev. Lett. **123**, 214301 (2019).
[25] B.-I. Popa and S. A. Cummer, Nat. Commun. **5**, 158702 (2014).
[26] V. F. Nesterenko, C. Daraio, E. B. Herbold, and S. Jin, Phys. Rev. Lett. **95**, 158702 (2005).
[27] B. Liang, B. Yuan, and J. C. Cheng, Phys. Rev. Lett. **103**, 104301 (2009).
[28] N. Boechler, G. Theocharis, and C. Daraio, Nat. Mater. **10**, 665 (2011).
[29] F. Li, P. Anzel, J. Yang, P. G. Kevrekidis, and C. Daraio, Nat. Commun. **5**, 5311 (2014).
[30] B. Liang, X. S. Guo, J. Tu, D. Zhang, and J. C. Cheng, Nat. Mater. **9**, 989 (2010).
[31] A. Kamal, A. Roy, J. Clarke, and M. H. Devoret, Phys. Rev. Lett. **113**, 247003 (2014).
[32] K. L. Johnson and K. L. Johnson, *Contact Mechanics* (Cambridge University Press, Cambridge, England, 1987).
[33] V. F. Nesterenko, *Dynamics of Heterogeneous Materials* (Springer, New York, 2001).
[34] C. Chong, M. A. Porter, P. G. Kevrekidis, and C. Daraio, J. Phys. Condens. Matter **29**, 413003 (2017).
[35] E. Kim, F. Li, C. Chong, G. Theocharis, J. Yang, and P. G. Kevrekidis, Phys. Rev. Lett. **114**, 118002 (2015).
[36] Y. Jang, S. Kim, E. Kim, and J. Rho, Sci. Bull. **70**, 1080 (2025).
[37] E. Kim, J. Yang, H. Hwang, and C. W. Shul, Int. J. Impact Eng. **101**, 24 (2017).
[38] R. Chaunsali, M. Toles, J. Yang, and E. Kim, J. Mech. Phys. Solids **107**, 21 (2017).
[39] Y. Jang, S. Kim, D. Lee, E. Kim, and J. Rho, Phys. Rev. Lett. **134**, 136901 (2025).
[40] E. Kim and J. Yang, J. Mech. Phys. Solids **71**, 33 (2014).
[41] D. J. Inman and R. C. Singh, *Engineering Vibration* (Prentice Hall Englewood Cliffs, NJ, 1994), Vol. 3.
[42] See Supplemental Material at http://link.aps.org/supplemental/10.1103/3n97-7kmd, which includes Refs. [23,24,27,32–35,43–48], for detailed descriptions of the experiments and data acquisition, discrete element model (including the dispersion relation of discrete cells and free vibration of a continuum beam), numerical simulation, linear wave dynamics (including boomerang-shaped waves and local wave amplification), and further investigation of nonlinear wave dynamics (including nonlinear spectrum maps and short-time Fourier transforms).
[43] Y. Jang, E. Kim, J. Yang, and J. Rho, Appl. Math. Model. **125**, 571 (2024).
[44] J. J. Xiao, K. Yakubo, and K. W. Yu, Phys. Rev. B **73**, 054201 (2006).
[45] M. J. Zheng, J. J. Xiao, and K. W. Yu, Phys. Rev. A **81**, 033829 (2010).
[46] K. H. Matlack, M. Serra-Garcia, A. Palermo, S. D. Huber, and C. Daraio, Nat. Mater. **17**, 323 (2018).
[47] B. R. Mace and E. Manconi, J. Acoust. Soc. Am. **131**, 1015 (2012).
[48] R. E. D. Bishop, J. R. Aeronaut. Soc. **59**, 781 (1955).
[49] K. L. Tsakmakidis, A. D. Boardman, and O. Hess, Nature (London) **450**, 397 (2007).
[50] L. G. Bennetts, M. A. Peter, and R. V. Craster, J. Fluid Mech. **854**, R4 (2018).
[51] V. Romero-García, R. Picó, A. Cebrecos, V. J. Sánchez-Morcillo, and K. Staliunas, Appl. Phys. Lett. **102**, 091906 (2013).
[52] N. Yang, N. Li, L. Wang, and B. Li, Phys. Rev. B **76**, 020301(R) (2007).
[53] M. Kauranen and A. V. Zayats, Nat. Photonics **6**, 737 (2012).
[54] L. Novotny, Am. J. Phys. **78**, 1199 (2010).
[55] D. N. Basov, M. M. Fogler, and F. J. García de Abajo, Science **354**, aag1992 (2016).